nature neuroscience

Pathway-specific reorganization of projection neurons in somatosensory cortex during learning

Jerry L Chen[1], David J Margolis[1,2,5], Atanas Stankov[1,3], Lazar T Sumanovski[1], Bernard L Schneider[4] & Fritjof Helmchen[1,2]

In the mammalian brain, sensory cortices exhibit plasticity during task learning, but how this alters information transferred between connected cortical areas remains unknown. We found that divergent subpopulations of cortico-cortical neurons in mouse whisker primary somatosensory cortex (S1) undergo functional changes reflecting learned behavior. We chronically imaged activity of S1 neurons projecting to secondary somatosensory (S2) or primary motor (M1) cortex in mice learning a texture discrimination task. Mice adopted an active whisking strategy that enhanced texture-related whisker kinematics, correlating with task performance. M1-projecting neurons reliably encoded basic kinematics features, and an additional subset of touch-related neurons was recruited that persisted past training. The number of S2-projecting touch neurons remained constant, but improved their discrimination of trial types through reorganization while developing activity patterns capable of discriminating the animal's decision. We propose that learning-related changes in S1 enhance sensory representations in a pathway-specific manner, providing downstream areas with task-relevant information for behavior.

Activity in the barrel field of S1 reflects tactile stimuli to the facial whiskers, but is also modulated by behavioral state, movement, motor-related neural activity and reward contingency[1–5]. Such information processed in S1 is transferred to other brain areas through excitatory long-range projection neurons. In layer 2/3 (L2/3) of S1, cortico-cortical neurons predominate[6] with M1-projecting (M1P) and S2-projecting (S2P) neurons representing two large, non-overlapping subpopulations[7–10]. Previous studies have demonstrated that these two subpopulations differ functionally in their intrinsic excitability and in their responses to whisker stimulation during both anesthetized and awake conditions[9,10]. In trained mice performing whisker-based discrimination tasks, we found that S2P and M1P neurons functionally differ in a task-dependent manner: S2P neurons were prominently recruited and more relevant during texture discrimination, whereas M1P neurons showed increased responsiveness and discriminative power during object localization[8]. Thus, S1 is capable of conveying different streams of information to M1 and S2 during task performance.

What do these two pathways encode during a task and how does their activity evolve from a naive to a trained animal? Do the emerging activity patterns reflect the acquisition of task-related behavior? Are there additional changes in S1 that persist even when the animal is not performing the task? To address these questions, we monitored changes in mouse behavior over the course of texture discrimination learning and used *in vivo* two-photon calcium imaging to longitudinally measure touch-evoked, task-related activity in S2P and M1P neurons. Our results indicate that different activity patterns emerge in each pathway during task learning. M1P neurons reliably and cumulatively encoded whisker-touch events, whereas S2P neurons acquired decision-related activity during learning. The emergence of selective information flow from one cortical region to connected regions may represent an essential part of mesoscale brain dynamics driving learned behavior.

RESULTS

Behavioral correlates of texture discrimination learning

We trained seven mice to perform a head-fixed go/no-go texture discrimination task. Animals had to lick for a water reward when presented with a target texture, a panel of coarse sandpaper (P100, 'hits' on go trials), and withhold licking when presented with a smoother non-target texture (P1200, 'correct rejections' on no-go trials; **Fig. 1a–c**). 'Misses' on go trials were not rewarded. In our previous study[8], 'false alarms' on no-go trials were punished with an air puff against the whisker pad and a time out period. Here, only a time out period was used to avoid contaminating neuronal activity by air puff–driven whisker deflections, allowing us to compare texture-touch activity between correct rejection and false alarm trials. To determine whether learning-related changes in S1 persist outside of task conditions, we also subjected mice to pre-training and post-training sessions, in which textures were presented without reward or punishment.

We first identified behavioral correlates of task learning by quantifying licking rate and whisking amplitude obtained from lick sensor measurements and high-speed videography, respectively. Mice displayed different learning rates, achieving saturating performance levels in 3–10 sessions, which were maintained thereafter.

[1]Brain Research Institute, University of Zurich, Zurich, Switzerland. [2]Neuroscience Center Zurich, University of Zurich/ETH Zurich, Zurich, Switzerland. [3]Institute of Neuroinformatics, University of Zurich/ETH Zurich, Zurich, Switzerland. [4]Brain Mind Institute, EPFL, Lausanne, Switzerland. [5]Present address: Department of Cell Biology and Neuroscience, Rutgers University, New Brunswick, New Jersey, USA. Correspondence should be addressed to F.H. (helmchen@hifo.uzh.ch).

Received 25 February; accepted 27 May; published online 22 June 2015; doi:10.1038/nn.4046

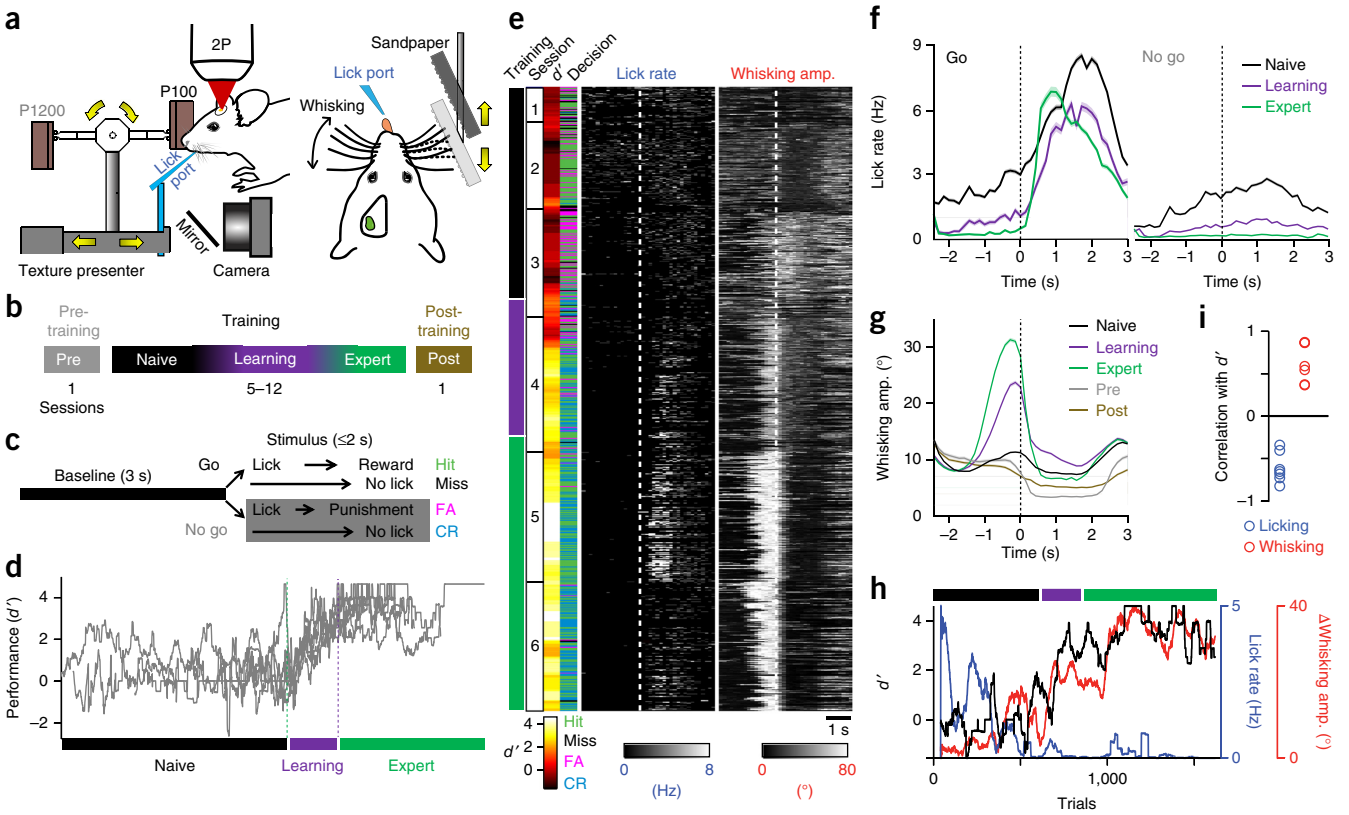

Figure 1 Behavior correlates of learning a texture discrimination task. (**a**) Behavior setup. (**b**) Experimental time course. (**c**) Trial structure for go/no-go texture discrimination task. (**d**) Overlaid learning curves (*d′*) for individual animals, normalized and aligned to learning onset and completion (**Supplementary Fig. 1**). (**e**) Single-trial measurements of lick rate and whisking amplitude from an example animal across training aligned to time of first texture touch (dotted line). Corresponding session number, training phase, *d′* and decision are also shown. (**f**) Time course of lick rate aligned to first touch within go trials (left) and no-go trials (right) across different training periods (solid line, mean; shaded area, s.e.m.). (**g**) Time course of whisking amplitude aligned to first touch across different training periods. (**h**) Learning curve (black) for animal in **e** plotted against average pre-stimulus lick rate (blue) and average pre-stimulus whisking amplitude (red). (**i**) Cross-correlation across trials of learning curve to average pre-stimulus lick rate (blue) or average pre-stimulus whisking amplitude (red) for individual animals (solid line, mean; shaded area, s.e.m.; $n = 13{,}715$ trials, 7 animals).

To compare across animals, we applied a state-space model[11] to define three phases in each animal: an initial naive phase of training where animals performed at near chance levels, a learning phase in which performance increased and an expert phase where performance saturated (**Fig. 1d** and **Supplementary Fig. 1**). The naive phase varied greatly in duration across animals (~300–3,000 trials), whereas the learning phase only spanned ~200–700 trials. During the naive phase, mice exhibited licking distributed throughout the trial period for both go and no-go trials (**Fig. 1e**,**f**). During learning, licking before texture presentation decreased across both trial types. Improved task performance reflected a gradual suppression of licking during no-go trials, reducing false alarms, whereas licking persisted following texture presentation for go trials (**Supplementary Fig. 2**). In expert sessions, mice exhibited a mean reaction time from touch to first lick of 502 ± 8 ms during hit trials. Only a small fraction of all trials across the entire training period were miss trials (6.4 ± 2.0%, $n = 7$ animals).

In addition to licking behavior changes, whisking behavior also evolved throughout training. In naive sessions, low-amplitude whisking occurred throughout the trial period (**Fig. 1e**,**g** and **Supplementary Fig. 3a**,**b**). As training proceeded, mice adopted a well-timed, high-amplitude rhythmic whisking behavior in response to audio cues that accompanied texture presentation. Whisking amplitude increased in the second before, and through, initial texture touch, and decreased thereafter (**Fig. 1e**,**g**), resulting in different sweep patterns of the principal whisker against the texture across training (**Supplementary Fig. 3c**,**d**). This stereotyped, anticipatory whisking occurred in all mice and was not observed during pre- and post-training sessions, suggesting that this behavior is related to task engagement. Pre-contact whisking amplitude became larger and was positively correlated with increased task performance, whereas pre-contact licking decreased and was negatively correlated (**Fig. 1h** and **Supplementary Fig. 1**). These results indicate that mice adopt specific motor strategies for texture discrimination performance during learning.

Kinematic features of texture discrimination

Given that increased whisking correlated with improved performance during training, we investigated how this self-induced motion changed the physical interaction of the principal whisker with textures during contact. We analyzed whisker kinematics across the first second of touch, as contact lasted for at least this duration (1.7 ± 0.6 s, mean ± s.d.) for the majority of training trials (~85%). Touch produced curvature changes ($|\Delta\kappa|_{max}$) reflecting contact forces of the whisker as it catches on surface irregularities, as well as high-velocity/high-acceleration 'stick-slip' events as it springs free (**Fig. 2a**)[12]. These two features can be physically coupled during touch, as $|\Delta\kappa|_{max}$ and stick-slip frequency were correlated on a trial-by-trial basis for both textures across training (**Supplementary Fig. 4a**). However, we also observed instances in which these features were not coupled.

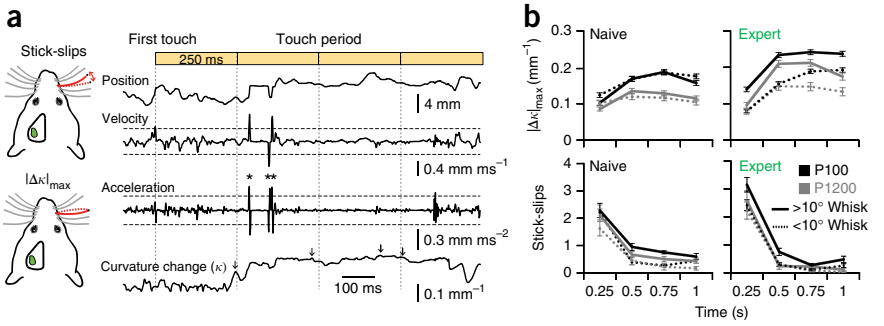

Figure 2 Active whisking increases stick-slip events. (**a**) Diagram of whisker kinematics (left) with example single-trial measurements of stick-slips (*) and maximum curvature change (arrows) identified per 250-ms bin (right). (**b**) Maximum curvature change ($|\Delta\kappa|_{max}$, upper row) and number of stick-slip events (lower row) across the initial 1-s period after touch onset for P100 and P1200 textures according to pre-stimulus whisking amplitude in naive (left) and expert (right) training trials. Error bars represent s.e.m. $n = 4{,}336$ trials, 5 animals.

A substantial fraction of trials displayed zero stick-slip events for the principal whisker with a large range of $|\Delta\kappa|_{max}$ across both textures. On trials without principal whisker stick-slip events, the animal's expert performance was lower compared with trials with stick-slip events (**Supplementary Fig. 4b**), indicating that stick-slip events from the principal whisker improve texture discrimination.

In the absence of principal whisker stick-slip events, expert performance was still higher than naive performance ($P < 0.02$, one-tailed paired Student's t test; **Supplementary Fig. 4b**). Although stick-slip events from surrounding whiskers (not measured here) could contribute to the elevated performance level in such trials, another possibility is that other independent features, such as $|\Delta\kappa|_{max}$, might also be informative for texture discrimination. We therefore looked at $|\Delta\kappa|_{max}$ of the principal whisker during P100 and P1200 texture contacts across training, sorted by trials with high- versus low-amplitude whisking. Overall, $|\Delta\kappa|_{max}$ was larger in high-amplitude whisking trials, but $|\Delta\kappa|_{max}$ was larger for P100 than for P1200 texture in naive and expert phases, irrespective of whisking behavior ($P < 0.05$, one-way repeated-measures ANOVA; **Fig. 2b**). Receiver operating characteristic (ROC) analysis of $|\Delta\kappa|_{max}$ against texture identity revealed that this feature discriminated between P100 and P1200 textures above chance levels in both naive and expert phase (**Supplementary Fig. 4c**), suggesting that it could be used by animals for texture discrimination.

In contrast, differences in stick-slip events across textures depended on whisking amplitude. Only in high-amplitude whisking trials in expert animals did stick-slip events occur with greater frequency for P100 than P1200 textures ($P < 0.05$, one-way repeated-measures ANOVA) and could be used to discriminate textures above chance levels (**Supplementary Fig. 4c**). Both $|\Delta\kappa|_{max}$ and stick-slip frequency were larger during training than during pre- and post-training sessions, when whisking was infrequent ($P < 0.05$, one-way repeated-measures ANOVA; **Supplementary Fig. 4d**,**e**). Thus, although mice have the capacity to discriminate textures with $|\Delta\kappa|_{max}$ under non-whisking conditions, discrimination can be enhanced in expert mice by active whisking to increase differences in stick-slip frequency across textures[13–16].

Touch-related projection neurons across sessions

We next examined how S2P and M1P neuron properties evolved over the experimental time course. We identified M1P and S2P neurons using previously described methods[8] (**Fig. 3a**). Briefly, using adult transgenic Cre-dependent tdTomato reporter mice[17], we injected a retrograde-infecting adeno-associated virus (AAV, serotype 6) expressing Cre recombinase (AAV6-Cre)[6] into S2 to induce tdTomato expression in S2P neurons in S1. M1P neurons were labeled by M1 injection of cholera toxin subunit-B (CTB-Alexa647). Unlabeled (UNL) neurons likely consisted of a mixed population of unstained S2P or M1P neurons as well as neurons projecting to other cortical areas. In general, UNL neurons showed either intermediate responses between M1P and S2P neurons or responses more similar to one particular subtype (**Supplementary Figs. 5–10**). In addition, we injected into S1 an AAV1 expressing the genetically encoded calcium indicator yellow-cameleon Nano140 (YC-Nano140), a reporter of spiking-related calcium signals[18]. Neurons displayed heterogeneous calcium signals, with varying amplitudes and differences in trial-to-trial reliability, but with subsets clearly responding to touch with immediate and partially prolonged spiking activity (**Fig. 3a**). *In vivo* two-photon calcium imaging was performed across pre-training, training and post-training sessions, in which neurons were chronically followed throughout the experimental time course (**Fig. 3b**). To increase the number of neurons monitored per animal, we implemented a multi-plane imaging approach, in which two-dimensional frame scanning was performed in each trial, but the focal plane alternated between three pre-assigned imaging depths such that neuronal subsets at each depth were imaged once every three trials (**Supplementary Fig. 5**). Using this approach, we tracked calcium signals in 89–150 neurons per animal (mean: 101 per animal; total number of cells tracked: 707).

S1 neurons are primarily responsive to sensory input from whisker touch[19–21]. We first identified active neurons as those showing calcium signals that were significantly different from the surrounding neuropil signal. To identify 'touch' neurons that show activity related to texture contact, we cross-correlated cellular calcium signals for all active neurons across all trials in each session against a binary vector representing touch periods. Active neurons with no significant positive correlation to touch or with correlation peaks outside defined lag windows were classified as 'non-touch' (**Supplementary Fig. 6a–c**). Among these neurons, we also observed a small number of neurons whose activity correlated to whisking amplitude during active whisking[8,22] (data not shown), but classified these neurons as being non-touch for the purposes of this study.

Classification of individual neurons differed from session to session, indicating a certain degree of variability in neuronal responsiveness (**Fig. 3b** and **Supplementary Fig. 6d**). We first compared the fraction of touch and non-touch neurons across cell types over the experimental time course (**Fig. 3c** and **Supplementary Fig. 6e**). The fraction of touch neurons among all M1P neurons (including non-active ones) increased over the course of training from 13% for pre-training sessions to 21% in expert sessions ($P < 0.05$, one-tailed bootstrap test) and remained elevated at 27% for post-training sessions ($P < 0.05$, one-tailed bootstrap test), suggesting that training increases the sensitivity of M1P neurons to touch and persists beyond task engagement. In contrast, the fraction of S2P touch neurons remained unchanged. Notably, the fraction of S2P non-touch neurons decreased in expert sessions (2%), but increased again in post-training sessions (9%, $P < 0.05$, one-tailed bootstrap test). Consequently, the percentage of touch neurons among the active neuronal pool showed a significant peak for S2P neurons in expert mice ($P < 0.05$, one-tailed bootstrap test; **Supplementary Fig. 6f**). These results suggest

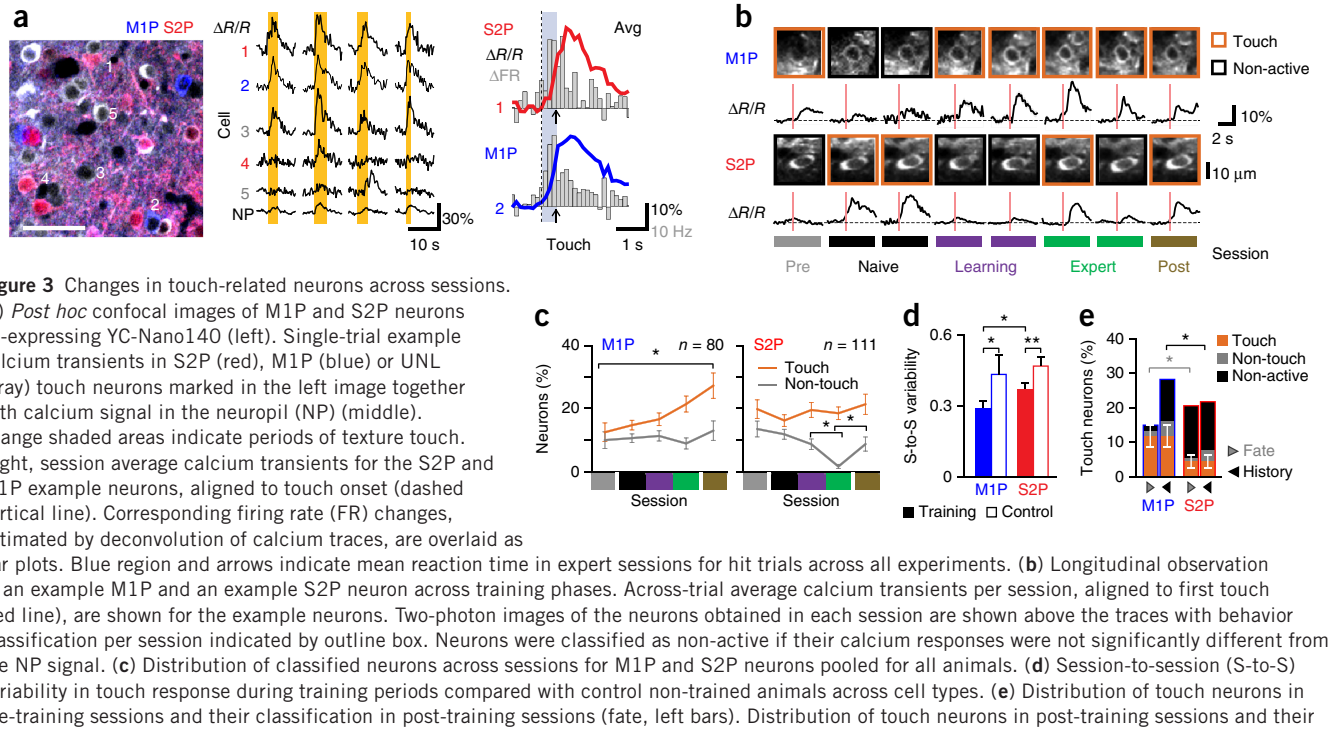

Figure 3 Changes in touch-related neurons across sessions. (**a**) *Post hoc* confocal images of M1P and S2P neurons co-expressing YC-Nano140 (left). Single-trial example calcium transients in S2P (red), M1P (blue) or UNL (gray) touch neurons marked in the left image together with calcium signal in the neuropil (NP) (middle). Orange shaded areas indicate periods of texture touch. Right, session average calcium transients for the S2P and M1P example neurons, aligned to touch onset (dashed vertical line). Corresponding firing rate (FR) changes, estimated by deconvolution of calcium traces, are overlaid as bar plots. Blue region and arrows indicate mean reaction time in expert sessions for hit trials across all experiments. (**b**) Longitudinal observation of an example M1P and an example S2P neuron across training phases. Across-trial average calcium transients per session, aligned to first touch (red line), are shown for the example neurons. Two-photon images of the neurons obtained in each session are shown above the traces with behavior classification per session indicated by outline box. Neurons were classified as non-active if their calcium responses were not significantly different from the NP signal. (**c**) Distribution of classified neurons across sessions for M1P and S2P neurons pooled for all animals. (**d**) Session-to-session (S-to-S) variability in touch response during training periods compared with control non-trained animals across cell types. (**e**) Distribution of touch neurons in pre-training sessions and their classification in post-training sessions (fate, left bars). Distribution of touch neurons in post-training sessions and their classification in pre-training sessions (history, right bars). Only neurons imaged across both sessions are shown. Error bars represent s.d. from bootstrap test (**c**,**e**) or s.e.m. (**d**). $n = 707$ neurons in 7 training animals, 369 neurons in 3 control animals; $^*P < 0.05$, $^{**}P < 0.02$, one-tailed bootstrap test.

that training improves the 'signal-to-background' of touch-related responses in S2P neurons during texture discrimination, which is restricted to periods of task engagement.

Although the fraction of cells responsive to touch increased in M1P neurons and remained steady in S2P neurons, these numbers could either reflect a subset of neurons that is mostly stable or a larger pool of neurons that varied in their response across sessions. To distinguish these alternatives, we quantified the session-to-session response variability, that is, the probability of neurons switching class from touch to either non-touch or non-active or vice versa. During training, S2P neurons were more variable in their response compared with M1P neurons (0.37 ± 0.03 versus 0.29 ± 0.03, mean ± s.e.m.; $P < 0.05$, one-way ANOVA, Tukey's *post hoc* test; **Fig. 3d** and **Supplementary Fig. 6g**). To determine whether this difference was a result of training or merely reflected the baseline response variability in these subtypes, we performed chronic imaging in control animals ($n = 3$ animals, 6 sessions per animal) that were not engaged in texture discrimination training. Notably, baseline response variability was consistently higher for each cell type than during training ($P < 0.05$, one-way ANOVA, Tukey's *post hoc* test; **Fig. 3d** and **Supplementary Fig. 6g**). Differences in response variability were not observed across subtypes in non-trained animals. This finding suggests that training reduces session-to-session response variability, most prominently in M1P neurons.

To examine the consequence of these changes in responsiveness following training, we also compared the 'fate' or 'history' of touch neurons between pre- and post-training sessions. We found that 80% of M1P touch neurons (12% of all M1P neurons) during pre-training

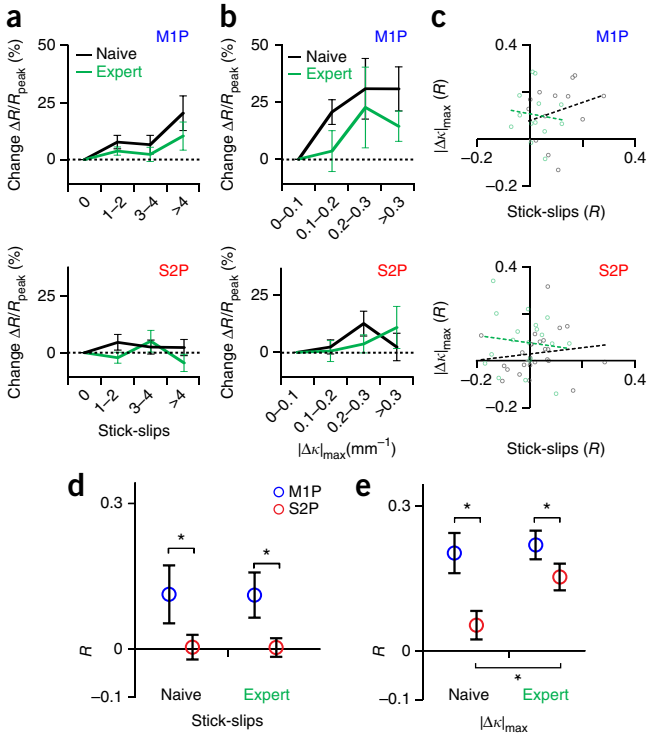

Figure 4 M1P neuron activity reliably encodes whisker kinematic features across learning. (**a**,**b**) Relative change in calcium transient peak amplitude with increasing stick-slip events (**a**) or $|\Delta\kappa|_{max}$ (**b**) according to cell type in naive and expert trials. Changes are quantified relative to $\Delta R/R$ amplitudes for zero stick-slip events and the smallest $|\Delta\kappa|_{max}$ bin, respectively. (**c**) Scatter plot of single neuron response correlations to $|\Delta\kappa|_{max}$ and stick-slip events across cell types in naive (black) and expert (green) trials. Linear regressions are shown (dotted lines). (**d**,**e**) Touch neuron correlation of mean calcium responses to stick-slip events (**d**) or $|\Delta\kappa|_{max}$ (**e**) in naive and expert trials across cell types. Error bars represent s.e.m. (**a**,**b**) and 95% confidence interval from permutation test (**d**,**e**). $n = 3,407$ trials, 307 touch neurons, 5 animals; $^*P < 0.05$, one-tailed bootstrap test.

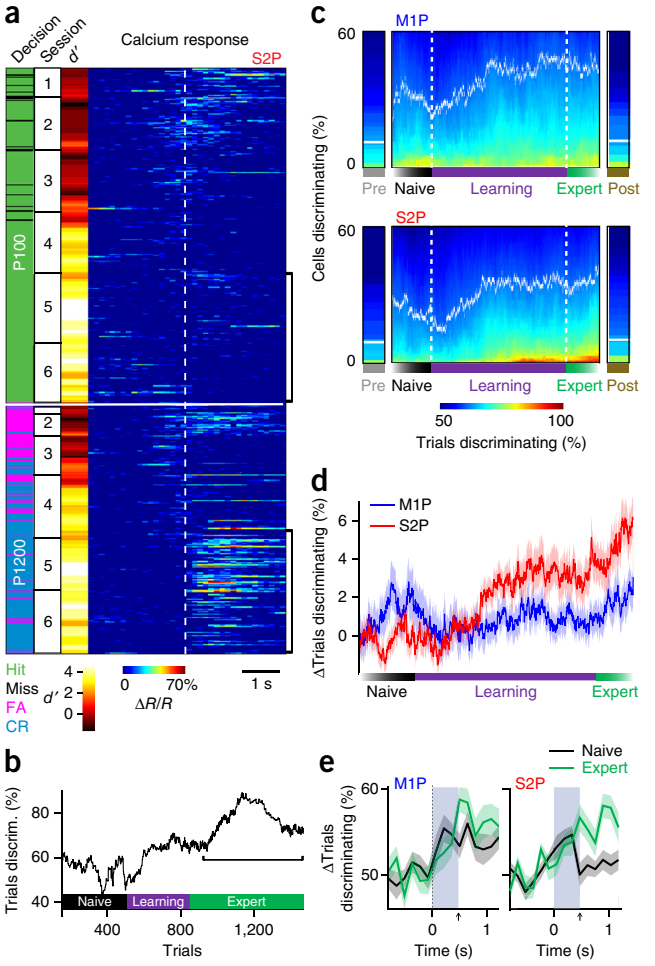

Figure 5 S2P neurons increase trial type discrimination during learning. (**a**) Single trial responses of example S2P touch neuron aligned to first touch (dotted line) sorted by texture and then by trial number. Corresponding session number and *d′* are also shown. This neuron acquires a selective response for no-go (P1200) trials in later phases of training. (**b**) Single-cell ROC analysis performed along a sliding window across training for the neuron shown in **a** for go versus no-go (P100 versus P1200) trials. Bar indicates trials with increased discriminative performance also shown in **a**. (**c**) Distribution of neurons discriminating go versus no-go (P100 versus P1200) trials across training by cell type obtained by sliding window single-cell ROC analysis. Trial times are aligned and normalized according to learning onset and completion (dotted white lines). Neurons are ranked according to fraction of trials discriminating (values indicated by color plot). Fraction of neurons discriminating above chance is indicated by solid white line, corresponding to 95th percentile of distribution from permutation test of trial labels. Fractions of neurons discriminating above chance for pre- and post-training sessions are shown on left and right, respectively. (**d**) Fraction of trials discriminating relative to naive phase during training across cell types. (**e**) ROC analysis across the 1-s periods before and following first touch in naive and expert trials across cell types. Blue region and arrow indicate mean reaction time in expert sessions for hit trials. Shaded area represents s.e.m. $n = 707$ neurons, 7 animals.

sessions were also classified as such in post-training sessions (**Fig. 3e** and **Supplementary Fig. 6h**). The increase in M1P touch neurons during training therefore predominantly represents a recruitment of previously inactive or non-touch neurons with little elimination of existing touch neurons. In contrast, a lower percentage of S2P pre-training touch neurons (22%, 5% of all S2P neurons) were also classified as such on post-training sessions ($P < 0.05$, one-tailed bootstrap test). In classifying the history of neurons, we found that only 21% of S2P touch neurons on post-training sessions were similarly classified on pre-training sessions, lower compared to M1P neurons ($P < 0.05$, one-tailed bootstrap test; **Fig. 3e** and **Supplementary Fig. 6h**). These results suggest that, although the number of S2P touch neurons remained similar, different sets of neurons were responsive before and after training. This could either reflect ongoing response variability or the selection of neurons with different tuning properties as investigated below.

M1P neurons encode kinematic features throughout learning

To determine whether neuronal activity related to basic whisker kinematics changed during learning, we first analyzed calcium responses with respect to stick-slip events and $|\Delta\kappa|_{max}$ in naive and expert phases of learning (**Supplementary Fig. 7a**). Given that sensory-evoked activity potentially relevant for learning occurs between touch onset and external reinforcement, we focused our time window of analysis to the first second of touch equivalent to the time to reward delivery on 'hit' trials (1.08 ± 0.41 s, mean ± s.d.) and punishment cues on 'false alarm' trials (1.09 ± 0.40 s). Higher firing rates in S1 neurons have been associated with both stick-slip events[13,14,23] and curvature changes[21,24]. Consistent with those findings, we found that the peak calcium response amplitude of M1P touch neurons increased with increasing number of stick-slip events and increasing $|\Delta\kappa|_{max}$ during naive and expert phases (**Fig. 4a**,**b** and **Supplementary Fig. 7b–d**). S2P neurons exhibited this response pattern for only $|\Delta\kappa|_{max}$ in expert trials.

Analysis of individual neuronal response correlation to kinematic features revealed that these features are encoded by mixed subpopulations with only a small degree of overlap (**Fig. 4c** and **Supplementary Fig. 7e**). Thus, a neuron that prefers curvature changes does not necessarily prefer stick-slip events. Although we observed S2P touch neurons with positive correlations for kinematic features, a large fraction also exhibited negative correlations. Overall, the population response of S2P neurons was not significantly correlated to stick-slip events during training (naive trials: $P = 0.06$, permutation test; expert trials: $P = 0.05$, permutation test), whereas M1P touch neurons consistently showed significant positive correlation ($P < 0.05$, permutation test; **Fig. 4d** and **Supplementary Fig. 7f**). All subtypes were significantly correlated with curvature changes, but M1P touch neurons showed higher correlation than S2P touch neurons throughout training ($P < 0.05$, one-tailed bootstrap test; **Fig. 4e**). Overall, this indicates that M1P touch neurons encode basic kinematic features throughout training.

S2P neurons switch preference for textures

Given the inconsistent responses of S2P neurons to kinematic features, we hypothesized that S2P neurons may either encode a higher order stimulus feature such as a general representation of the texture or a behavior-related aspect of the stimulus that develops during task learning. To test this, we analyzed neuronal responses according to texture or trial type. Some neurons developed selective responses for go or no-go trials across training (**Fig. 5a**). Single-neuron ROC analysis between go versus no-go (P100 versus P1200) trials, performed along a sliding window across training, indicated that neurons improved their trial type discrimination as mice reached expert performance (**Fig. 5b**). Fractions of neurons able to discriminate above chance levels increased for all cell types during learning (**Fig. 5c** and **Supplementary Fig. 8a–c**). This fraction was lower in both pre- and post-training sessions, indicating that increases in discriminative cells only occurred during task engagement ($P < 0.05$,

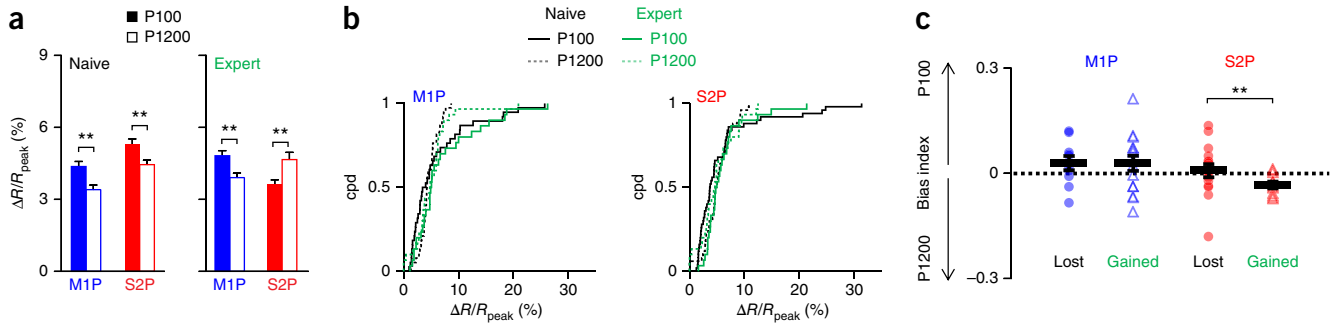

Figure 6 S2P neurons shift preference toward P1200-related trials. (**a**) Peak touch neuron calcium response across cell types for P100 versus P1200 trials in naive (left) and expert (right) session. (**b**) Cumulative probability distribution (cpd) of peak calcium response for touch neurons across cell types for P100 versus P1200 trials in naive and expert sessions. (**c**) Response preference for P100 versus P1200 trials in touch neurons lost after naive sessions or gained during expert sessions across cell types. Error bars represent s.e.m. $n = 411$ touch neurons, 7 animals; $^*P < 0.05$, $^{**}P < 0.001$, one-tailed Student's t test.

one-tailed bootstrap test). Although more M1P neurons could discriminate trial type above chance during training, the mean discrimination power of discriminative M1P neurons did not increase (**Fig. 5d**). The variance in discrimination power across these neurons also did not change, suggesting that, despite the increased numbers of discriminative M1P neurons, the distribution in the population response between the two trial types was unchanged (**Supplementary Fig. 8d**). Discriminative S2P neurons, in contrast, showed increased discrimination power from learning to expert sessions. This change was primarily the result of improvements in discrimination among the top-performing neurons (**Supplementary Fig. 8e**).

To examine whether these discriminative signals could arise in a relevant trial period to drive behavior, we performed single-neuron ROC analysis at each time point during the 1-s periods before and following touch onset (**Fig. 5e**). The discriminative power of both cell types increased immediately following touch onset through a period equivalent to the reaction time observed during hit trials in expert mice. However, in S2P neurons, we noticed that discriminative power continued to rise after this period in expert, but not naive, trials ($P < 0.05$, one-way repeated-measures ANOVA). This indicates that, although trial type differences in activity that is informative for behavior can emerge in these neurons, additional differences can also exist beyond the behavioral response.

To understand how S2P touch neurons' discrimination improves, we measured calcium responses for each texture. In naive trials, P100 texture (go trials) produced larger peak responses than P1200 texture (no-go trials) in both M1P and S2P touch neurons ($P < 0.001$, one-tailed Student's t test; **Fig. 6a** and **Supplementary Fig. 9a**). This finding is consistent with higher firing rates associated with rougher textures[13,14,23]. However, in expert trials, we found a lower peak response in S2P touch neurons for P100 compared with P1200 texture ($P < 0.001$, one-tailed Student's t test; **Fig. 6a** and **Supplementary Fig. 9b,c**). Analysis of the distribution of peak responses across these neurons revealed that the reduction in activity occurred in a subpopulation of neurons that responded highly to the P100 texture ($P < 0.05$, Kolmogorov-Smirnov test; **Fig. 6b** and **Supplementary Fig. 9d**). Given the session-to-session response variability observed in S2P neurons, we asked whether this variability related to the selection of subpopulations with different texture preferences. S2P touch neurons responsive in naive, but not expert, sessions preferred either P100 or P1200 textures, whereas neurons that were responsive in expert, but not naive, sessions predominantly displayed a preference for the P1200 texture ($P < 0.05$, one-tailed Student's t test; **Fig. 6c** and **Supplementary Fig. 9e**). In all cell types, touch neurons that were responsive in both naive and expert sessions did not consistently

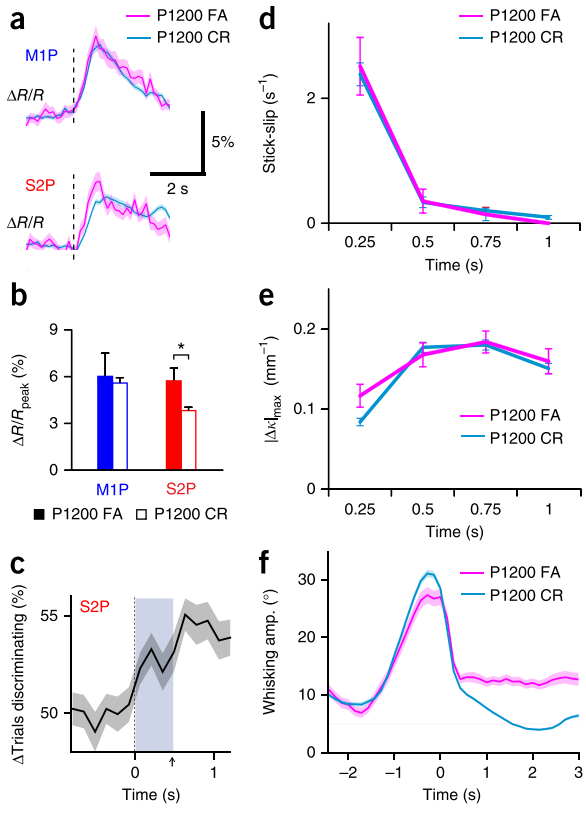

Figure 7 S2P neurons display decision-related activity in late phases of learning. (**a**) Average touch neuron calcium response to false alarm versus correct rejection in late learning to expert trials. (**b**) Peak touch neuron calcium response across cell types to false alarm versus correct rejection in late learning to expert trials. (**c**) ROC analysis for false alarm versus correct rejection trials across the 1-s periods before and following first touch in late learning to expert trials in S2P neurons. Blue region and arrow indicates mean reaction time in expert sessions for hit trials. (**d**) Stick-slip events across the first second after touch onset in false alarm versus correct rejection trials. (**e**) $|\Delta\kappa|_{max}$ across the first second after touch onset in false alarm versus correct rejection trials. (**f**) Time course of whisking amplitude aligned to first touch in false alarm versus correct rejection trials. Solid line represents mean, shaded area and error bars represent s.e.m. $n = 945$ trials, 7 animals; $^*P < 0.05$, one-tailed Student's t test.

change their preference (**Supplementary Fig. 9**). Overall, this suggests that the increased discrimination power of S2P neurons during training is achieved by a suppression of neurons preferring P100 trials and the recruitment of neurons preferring P1200 trials.

Training produces decision-related activity in S2P neurons

This change in preference of S2P touch neurons from P100 to P1200 textures may reflect modified sensory-evoked responses. Given the lack of correlation of their activity with texture-associated kinematics, we wondered whether this change may instead reflect a non-sensory, behavioral component. Given that mice learned to withhold their licking to the P1200 texture, we examined whether S2P touch neurons are modulated according to their decision by comparing correct rejection and false alarm trials during P1200 texture presentation. Larger calcium responses were observed for false alarm compared with correct rejection trials ($P < 0.05$, one-tailed Student's t test; **Fig. 7a**,**b** and **Supplementary Fig. 10**). Similar to what was observed between P100 versus P1200 trials, these differences in activity arise immediately following touch onset, persisting through and beyond the reaction time window (**Fig. 7c**). We found no significant difference in whisker kinematics or whisking behavior between these trial types, indicating that whisker touch occurred in the same manner ($P = 0.99$, stick-slip events; $P = 0.41$, $|\Delta\kappa|_{max}$; $P = 0.74$, whisking amplitude; one-way repeated-measures ANOVA; **Fig. 7d–f**). We observed no difference in activity between false alarm and correct rejection trials for M1P touch neurons ($P = 0.20$, one-tailed Student's t test), further supporting the notion that these neurons faithfully represent the sensory stimulus, agnostic of behavioral context. Taken together, these findings suggest that, unlike M1P neurons, S2P touch neuron responses could reflect the acquisition of a decision-associated sensory response during training.

DISCUSSION

In summary, we found that sensory-guided learning results in pathway-specific changes in the representation of tactile stimuli in S1, emerging in parallel with improvements in behavioral performance. During texture discrimination training, mice adopted a stereotyped, rhythmic whisking behavior that correlated with task performance and drove differences in stick-slip events between rough (P100) and smooth (P1200) textures. We found that curvature changes were also informative of texture identity independent of stick-slips events and did not require whisking. However, this expendability of whisking may merely reflect our experimental design in that the motion of the arriving texture during presentation against the head-fixed animal may be sufficient to deflect whiskers in a texture-dependent manner. Regardless, we speculate that the analyzed feature ($|\Delta\kappa|_{max}$) represents the resistance of the whisker against the texture related to the frictional properties of the surface[12]. Both curvature changes and stick-slip events can be used in combination to generate a percept of coarseness for texture discrimination. We speculate that active whisking specifically enhances texture-dependent stick-slip events to more efficiently extract texture information during behavior[15,23].

Increasing numbers of M1P neurons became responsive to touch over the course of training. The increased sensitivity to touch in M1P neurons persisted post-training and could be a result of a strengthening or disinhibition of feedforward responses in S1 (refs. 25–29). During this period the session-to-session response variability of M1P neurons was reduced compared to baseline conditions, suggesting that sensory representation in these neurons was stabilized. Indeed, despite the increase in the fraction of touch-related M1P neurons, we found no evidence for modification of response properties across the population in this subtype under behavioral conditions. M1P neurons reliably encoded texture-related kinematic features such as stick-slip events and curvature changes. Furthermore, they maintained a similar ability to discriminate P100 and P1200 textures across training. Whisker motion representation in M1 has also been found to be reliably encoded at a population-level during learning[30]; thus, sensorimotor integration across S1 and M1 maintains a faithful sensory representation that is stabilized by the recruitment of additional neurons during learning[26,31]. The adoption of active whisking strategies to physically drive relevant kinematics[13–16], and possibly an additional modulation of S1 by M1 activity during active whisking[2,32,33], might serve to improve the fidelity of this representation.

In contrast, S2P neurons undergo a different set of changes during texture discrimination learning. Although numbers of S2P touch neurons remain steady across training, there is a reduction of non-touch neurons. The increased bias toward touch versus non-touch neurons across active S2P neurons could improve the 'signal to background' of touch-related responses in this pathway. This difference was also observed in expert mice previously[8], although it should be noted that fewer non-touch neurons were identified here. Although the reasons for this discrepancy are unclear, some differences in experimental conditions, for example, the lack of air-puff punishment, could have altered associations with non-target textures across studies. In addition, data collection in our previous study occurred over a longer period of expert performance, throughout which the proportion of non-touch neurons continued to evolve with prolonged training (data not shown).

In addition to this shift in bias, the session-to-session response variability of S2P neurons during training, although lower than for non-training conditions, was still higher than for M1P neurons during training. Although it can be challenging to disambiguate response variability from active suppression or recruitment of different sets of neuronal pools, our analysis revealed that the latter partially occurred in S2P neurons during learning. S2P touch neurons improved their ability to discriminate between P100 and P1200 trials. We attributed this improvement to a shift in response preference toward P1200 trials by the suppression of P100-preferring neurons and the recruitment of P1200-preferring neurons. Although these responses were sensory evoked, they were modulated by behavioral context as S2P touch neurons became capable of discriminating between false alarm and correct rejection trials.

What underlies the functional differences observed between S2P and M1P neurons? Experiments in both anesthetized and awake, non-behaving animals have demonstrated that S2P and M1P neurons respond differently to tactile stimuli. In particular, M1P neurons showed adaptive firing to repetitive touches, whereas S2P neurons did not, suggesting that S2P neurons are well suited for integrating tactile information across time as might be required for texture discrimination[10]. S2P neurons did not respond to $|\Delta\kappa|_{max}$ and stick-slips as reliably as M1P neurons. Although our evidence suggests a task-related explanation for these differences, it does not exclude the possibility that S2P neurons might prefer other parameters of tactile information not considered here. Although intrinsic differences in sensory processing between M1P and S2P neurons may contribute by serving as initial biases that are enhanced during training, the trial type–specific responses in S2P neurons found in expert mice were not observed in post-training sessions, suggesting that they are neither intrinsic nor a result of persistent changes in S1 and therefore depend on behavioral state. The acquisition of decision-related activity in S2P neurons supports this notion. Differences in activity across trial types emerge immediately following touch and increase through the

animal's response, suggesting that these neurons have the capacity to drive decision-making in a bottom-up manner. At the same time, one cannot rule out the possibility that these signals merely reflect the animal's decision through top-down sources as described previously[34], as the discriminative power of S2P neurons persist beyond the reaction time specifically during expert trials. Our finding that S2P neuron activity was larger in false alarm compared with correct rejection trials and was lower for P100 trials than for P1200 trials argues against the simple explanation that S2P neurons carry an incorrect sensory representation similar to the P100 texture that results in the wrong behavioral response. Rather, our data suggest that, during learning, sensory activity in S2P neurons might increasingly become modulated by non-whisking–related feedback input[1], suppressing non-relevant activity and integrating contextual information on the basis of prior experience[35,36]. In non-human primates, S2 has been demonstrated to encode decision-related activity during a tactile discrimination task[37]. Our findings suggest that decision-related sensory activity may arise from interactions between S1 and S2.

In conclusion, we propose that the changes in neuronal pathway activity described in this study relate to procedural learning, in which a percept becomes linked to an action, as opposed to perceptual learning, which results in an improved ability to discriminate closely related stimuli. These modifications in S1 serve to both route specific information to downstream areas and refine sensory representations in specific pathways that are relevant for executing behavior.

METHODS

Methods and any associated references are available in the online version of the paper.

Note: Any Supplementary Information and Source Data files are available in the online version of the paper.

ACKNOWLEDGMENTS

We thank A. Iqbal for assistance with data analysis, and A. Ayaz, L. Egolf, S. Hofer, T. Mrsic-Flogel and S. Sachidhanandam for comments on the manuscript. This work was supported by a Swiss National Science Foundation (SNSF) grant (310030-127091 to F.H.), the Swiss SystemsX.ch initiative (project 2008/2011-Neurochoice to F.H. and B.L.S.), a SNSF Sinergia grant to F.H. and B.L.S. (CRSII3_147660/1), an AMBIZIONE grant from the SNSF to D.J.M. (PZ00P3_143232), a Forschungskredit of the University of Zurich (grant 541541808 to J.L.C.), and a fellowship from the US National Science Foundation, International Research Fellowship Program (grant 1158914 to J.L.C.).

AUTHOR CONTRIBUTIONS

J.L.C., D.J.M. and F.H. designed the study. J.L.C. and D.J.M. performed the experiments. J.L.C., A.S., L.T.S. and F.H. performed data analysis. B.L.S. contributed viral reagents. J.L.C. and F.H. wrote the paper.

COMPETING FINANCIAL INTERESTS

The authors declare no competing financial interests.

1. Pais-Vieira, M., Lebedev, M.A., Wiest, M.C. & Nicolelis, M.A. Simultaneous top-down modulation of the primary somatosensory cortex and thalamic nuclei during active tactile discrimination. *J. Neurosci.* **33**, 4076–4093 (2013).
2. Zagha, E., Casale, A.E., Sachdev, R.N., McGinley, M.J. & McCormick, D.A. Motor cortex feedback influences sensory processing by modulating network state. *Neuron* **79**, 567–578 (2013).
3. Gutierrez, R., Simon, S.A. & Nicolelis, M.A. Licking-induced synchrony in the taste-reward circuit improves cue discrimination during learning. *J. Neurosci.* **30**, 287–303 (2010).
4. Pantoja, J. *et al.* Neuronal activity in the primary somatosensory thalamocortical loop is modulated by reward contingency during tactile discrimination. *J. Neurosci.* **27**, 10608–10620 (2007).
5. Fanselow, E.E. & Nicolelis, M.A. Behavioral modulation of tactile responses in the rat somatosensory system. *J. Neurosci.* **19**, 7603–7616 (1999).
6. Aronoff, R. *et al.* Long-range connectivity of mouse primary somatosensory barrel cortex. *Eur. J. Neurosci.* **31**, 2221–2233 (2010).
7. Alloway, K.D., Lou, L., Nwabueze-Ogbo, F. & Chakrabarti, S. Topography of cortical projections to the dorsolateral neostriatum in rats: multiple overlapping sensorimotor pathways. *J. Comp. Neurol.* **499**, 33–48 (2006).
8. Chen, J.L., Carta, S., Soldado-Magraner, J., Schneider, B.L. & Helmchen, F. Behavior-dependent recruitment of long-range projection neurons in somatosensory cortex. *Nature* **499**, 336–340 (2013).
9. Sato, T.R. & Svoboda, K. The functional properties of barrel cortex neurons projecting to the primary motor cortex. *J. Neurosci.* **30**, 4256–4260 (2010).
10. Yamashita, T. *et al.* Membrane potential dynamics of neocortical projection neurons driving target-specific signals. *Neuron* **80**, 1477–1490 (2013).
11. Smith, A.C. *et al.* Dynamic analysis of learning in behavioral experiments. *J. Neurosci.* **24**, 447–461 (2004).
12. Boubenec, Y., Shulz, D.E. & Debregeas, G. Whisker encoding of mechanical events during active tactile exploration. *Front. Behav. Neurosci.* **6**, 74 (2012).
13. Arabzadeh, E., Zorzin, E. & Diamond, M.E. Neuronal encoding of texture in the whisker sensory pathway. *PLoS Biol.* **3**, e17 (2005).
14. von Heimendahl, M., Itskov, P.M., Arabzadeh, E. & Diamond, M.E. Neuronal activity in rat barrel cortex underlying texture discrimination. *PLoS Biol.* **5**, e305 (2007).
15. Wolfe, J. *et al.* Texture coding in the rat whisker system: slip-stick versus differential resonance. *PLoS Biol.* **6**, e215 (2008).
16. Zuo, Y., Perkon, I. & Diamond, M.E. Whisking and whisker kinematics during a texture classification task. *Phil. Trans. R. Soc. Lond. B* **366**, 3058–3069 (2011).
17. Madisen, L. *et al.* A robust and high-throughput Cre reporting and characterization system for the whole mouse brain. *Nat. Neurosci.* **13**, 133–140 (2010).
18. Horikawa, K. *et al.* Spontaneous network activity visualized by ultrasensitive Ca^{2+} indicators, yellow Cameleon-Nano. *Nat. Methods* **7**, 729–732 (2010).
19. Curtis, J.C. & Kleinfeld, D. Phase-to-rate transformations encode touch in cortical neurons of a scanning sensorimotor system. *Nat. Neurosci.* **12**, 492–501 (2009).
20. de Kock, C.P., Bruno, R.M., Spors, H. & Sakmann, B. Layer- and cell type–specific suprathreshold stimulus representation in rat primary somatosensory cortex. *J. Physiol. (Lond.)* **581**, 139–154 (2007).
21. O'Connor, D.H., Peron, S.P., Huber, D. & Svoboda, K. Neural activity in barrel cortex underlying vibrissa-based object localization in mice. *Neuron* **67**, 1048–1061 (2010).
22. Fee, M.S., Mitra, P.P. & Kleinfeld, D. Central versus peripheral determinants of patterned spike activity in rat vibrissa cortex during whisking. *J. Neurophysiol.* **78**, 1144–1149 (1997).
23. Jadhav, S.P., Wolfe, J. & Feldman, D.E. Sparse temporal coding of elementary tactile features during active whisker sensation. *Nat. Neurosci.* **12**, 792–800 (2009).
24. Xu, N.L. *et al.* Nonlinear dendritic integration of sensory and motor input during an active sensing task. *Nature* **492**, 247–251 (2012).
25. Gambino, F. & Holtmaat, A. Spike-timing-dependent potentiation of sensory surround in the somatosensory cortex is facilitated by deprivation-mediated disinhibition. *Neuron* **75**, 490–502 (2012).
26. Guic, E., Carrasco, X., Rodriguez, E., Robles, I. & Merzenich, M.M. Plasticity in primary somatosensory cortex resulting from environmentally enriched stimulation and sensory discrimination training. *Biol. Res.* **41**, 425–437 (2008).
27. Kuhlman, S.J., O'Connor, D.H., Fox, K. & Svoboda, K. Structural plasticity within the barrel cortex during initial phases of whisker-dependent learning. *J. Neurosci.* **34**, 6078–6083 (2014).
28. House, D.R., Elstrott, J., Koh, E., Chung, J. & Feldman, D.E. Parallel regulation of feedforward inhibition and excitation during whisker map plasticity. *Neuron* **72**, 819–831 (2011).
29. Gambino, F. *et al.* Sensory-evoked LTP driven by dendritic plateau potentials *in vivo*. *Nature* **515**, 116–119 (2014).
30. Huber, D. *et al.* Multiple dynamic representations in the motor cortex during sensorimotor learning. *Nature* **484**, 473–478 (2012).
31. Wiest, M.C., Thomson, E., Pantoja, J. & Nicolelis, M.A. Changes in S1 neural responses during tactile discrimination learning. *J. Neurophysiol.* **104**, 300–312 (2010).
32. Petreanu, L. *et al.* Activity in motor-sensory projections reveals distributed coding in somatosensation. *Nature* **489**, 299–303 (2012).
33. Lee, S., Kruglikov, I., Huang, Z.J., Fishell, G. & Rudy, B. A disinhibitory circuit mediates motor integration in the somatosensory cortex. *Nat. Neurosci.* **16**, 1662–1670 (2013).
34. Nienborg, H. & Cumming, B.G. Decision-related activity in sensory neurons reflects more than a neuron's causal effect. *Nature* **459**, 89–92 (2009).
35. Romo, R., Lemus, L. & de Lafuente, V. Sense, memory and decision-making in the somatosensory cortical network. *Curr. Opin. Neurobiol.* **22**, 914–919 (2012).
36. Diamond, M.E. & Arabzadeh, E. Whisker sensory system: from receptor to decision. *Prog. Neurobiol.* **103**, 28–40 (2013).
37. Romo, R., Hernandez, A., Zainos, A., Lemus, L. & Brody, C.D. Neuronal correlates of decision-making in secondary somatosensory cortex. *Nat. Neurosci.* **5**, 1217–1225 (2002).

ONLINE METHODS

Generation of viruses. AAV-pgk-Cre and AAV-EF1α-YC-Nano140 constructs were previously described[6,8]. Recombinant serotype 6 AAV particles were produced by co-transfecting AAV-293 cells with the shuttle plasmid and the pDP6 packaging plasmid. Recombinant serotype 1 AAV particles were produced by co-transfecting AAV-293 cells with the shuttle plasmid and the pDF1 packaging plasmid. Cell lysates were subjected to purification on iodixanol density gradients followed by HPLC with HiTrap Heparin column for AAV6 or by anion exchange HPLC for AAV1 (GE Healthcare Bio-Sciences AB) using standard procedures. The viral suspension obtained was concentrated using Centricon centrifugal filter devices with a molecular weight cut-off of 100 kDa (Millipore), and the suspension medium replaced with PBS. Vector titers were determined by measuring the number of encapsidated genomes per ml by real-time PCR.

Viral and tracer injections. Experimental procedures followed the guidelines of the Veterinary Office of Switzerland and were approved by the Cantonal Veterinary Office in Zurich. Stereotaxic viral and tracer injections were performed on young adult (P35–42) male transgenic Cre-dependent tdTomato reporter mice (ROSA26tm14(CAG-tdTomato), Ai14) as previously described[8]. AAV1-EF1α-YC-Nano140 (300 nl, ~1×10^9 vg μl^{-1}) was delivered into S1, targeting L2/3 (1.1 mm posterior to bregma, 3.3 mm lateral, ~300 µm below the pial surface). AAV6-pgk-Cre (300 nl, ~1×10^9 vg μl^{-1}) was delivered into S2, targeting L2/3 and L5 (0.7 mm posterior to bregma, 4.2 mm lateral, ~300 and 500 µm below the pial surface). CTB-Alexa647 (Molecular Probes, Invitrogen; 300 nl, 1%, wt/vol) was injected into M1 immediately following the last behavior imaging session, targeting L2/3 and L5 (1.2 mm anterior to bregma, 0.6 mm lateral, ~300 and 500 µm below the pial surface).

Cranial window implantation and habituation. To allow long-term *in vivo* calcium imaging, a cranial window was implanted 24 h after virus injections over S1 as described[8]. A metal post for head fixation was implanted on the skull, contralateral to the cranial window, using dental acrylic. Mice were subsequently housed, 1–4 animals per cage, in reverse light/dark cycle (12 h/12 h) rooms with all remaining experimental procedures performed during animal's dark period. One week following chronic window implantation, mice were handled daily for 1 week while acclimated to a minimum of 15 min of head fixation. Mice were water restricted for training sessions but not for pre- and post-training sessions.

Texture discrimination task. Behavior experiments were performed using a data acquisition interface (USB-6008, National Instruments) and custom-written LabVIEW software (National Instruments) to control devices required for the task and for recording trial and licking data. Behavior was reported by licking of a water port mounted to a piezo film sensor (MSP1006-ND, Measurement Specialties) triggering delivery of water (5–6 µl) through a miniature rocker solenoid valve (0127; Buerkert). Mice were initially trained for two sessions to reliably trigger water by licking the lick port and then proceeded to texture discrimination training. Commercial-grade sandpaper (3M) was used where rough sandpaper (P100) served as go-stimulus and smooth sandpaper (P1200) served as no-go stimulus. Sandpapers were mounted onto panels attached to a stepper motor (T-NM17A04, Zaber) mounted onto a motorized linear stage (T-LSM100A, Zaber) to move textures in and out of reach of whiskers. During initial task training, go trials were presented with 90% probability relative to no-go trials to acclimate mice to reward retrieval associated with texture presentation. Over the course of the first 1–2 sessions, this probability was gradually decreased to 50% probability for each trial type with a maximum of three consecutive presentations of the same trial type. A trial consisted of a 3-s pre-stimulus period followed by stimulus presentation for a maximum of 2 s accompanied by an intermittent 2,093-Hz auditory cue tone. Licking during target stimulus presentation was scored as a 'hit' and triggered immediate withdrawal of the stimulus accompanied by water delivery paired with a 2,093/2,793-Hz auditory reward tone. A no lick was scored as a 'miss' whereby the next trial immediately followed. During presentation of the no-go texture, a no lick was scored as a 'correct rejection' (CR) whereby the next trial immediately followed; licking on no-go trials was scored as a 'false alarm' (FA), in which case the stimulus was immediately withdrawn, no water reward was given, and the animal was punished with a 12-s time out period accompanied by auditory white noise. Imaging during training proceeded until animals reached a performance level of greater than 80–85% correct and then followed for another two sessions. All training and imaging sessions occurred twice per day. Additional sandpapers of intermediate smoothness (P280, P600) were also presented as non-target stimuli during pre-training, post-training and expert sessions but were not analyzed. For training experiments, seven mice were used in this study with an additional three mice excluded as they were unable to learn the task within 12 sessions. For control experiments, three mice were imaged for six sessions each under the same trial structure conditions but with the water port removed and with no reward or punishment accompanying texture presentation. Given that animals constituted a single experiment group that was chronically monitored, data collection was not randomized.

Intrinsic signal optical imaging. The S1 barrel column corresponding to the YC-Nano140 expression area was identified using intrinsic signal optical imaging under ~1.5% isoflurane anesthesia. The cortical surface was illuminated with 630-nm LED light, single whiskers were stimulated (2–4° rostro-caudal deflections at 10 Hz), and reflectance images were collected through a 4× objective with a CCD camera (Toshiba TELI CS3960DCL; 12-bit, 3-pixel binning, 427 × 347 binned pixels, 8.6-µm pixel size, 10-Hz frame rate). Intrinsic signal changes were computed as fractional changes in reflectance relative to the pre-stimulus average (50 frames; expressed as $\Delta R/R_{IOS}$). Barrel column centers for stimulated whiskers were located by averaging intrinsic signals (15 trials), median-filtering (5-pixel radius), and thresholding to find signal minima. Reference surface vasculature images were obtained using 546-nm LED illumination and matched to images acquired during two-photon imaging. Prior to behavior training, all whiskers excluding the principal and first-order surround whiskers corresponding to the expression area were partially trimmed to a length out of reach from texture contact during the task. During whisker trimming, the principal whisker was noted by images taken from the high-speed video camera for re-identification in subsequent imaging sessions for whisker tracking.

Two-photon imaging. We used a custom-built two-photon microscope controlled by HelioScan[38], equipped with a Ti:sapphire laser system (~100-fs laser pulses, Mai Tai HP, Newport Spectra Physics), a water-immersion objective (40 LUMPlanFl/IR, 0.8 NA; Olympus), galvanometric scan mirrors (model 6210; Cambridge Technology), and a Pockel's Cell (Conoptics) for laser intensity modulation. An electrically-tunable lens (ETL; EL-C-10-30-VIS-LD, tuned to a range of +50- to +200-mm focal length, 10-mm clear aperture, Optotune AG) was installed at the rear aperture of the microscope objective, together with an offset lens (LC4232, −100-mm focal length fused silica lens, Thorlabs)[39]. The ETL was controlled by a custom current controller delivering a stable current output from 0 to 200 mA at a maximum of 5 V. The behavior data acquisition interface provided an analog voltage signal (0–10V) to the ETL controller for between-trial focusing and, in ~20% of training sessions, for online correction of lick-related movement artifacts[40]. For initial identification of YC-Nano140–expressing and tdTomato-positive S2P neurons, a volume stack was acquired using 800-nm excitation and yellow (542/50 nm) and red (610/75 nm) emission filters, respectively (AHF Analysentechnik). For calcium imaging, YC-Nano140 was excited at 840 nm and fluorescence collected with blue (480/60 nm) and yellow (542/50 nm) emission filters. Images were acquired at 7 Hz with 256 × 128 pixel resolution. Single trials of 6–7-s duration were recorded at a time with 1-s breaks in between trials to allow for hard disk storage during inter-trial interval periods.

Whisker tracking. The whisker field was illuminated with 940-nm infrared LED light and movies were acquired at 500 Hz (500 × 500 pixels) using a high-speed CMOS camera (A504k; Basler). Average whisker angle across all imaged whiskers was measured using automated whisker tracking software[41]. Whisking amplitude was used as a measure to represent both rhythmic and non-rhythmic forms of whisking behavior. The envelope of whisking amplitude was calculated as the difference in maximum and minimum whisker angle along a sliding window equal to the imaging frame duration (142 ms). Rhythmic whisking power was determined by computing the power spectral density at 7–10 Hz for the average whisker angle along a sliding window equal to the imaging frame duration (142 ms). For all trials, the first and last possible time point for whisker to texture contact was quantified manually through visual inspection. For a random subset of trials

(~50% of all trials in 5 mice), the position of the principal whisker tip was manually tracked over a 1100-ms time period starting 100 ms preceding the initial touch using custom software (LabVIEW). Whisker tracking was performed blind according to the texture presented in each trial. For 2 mice, the principal whisker tip position was not analyzed due to improper focusing or field of view selection, which precluded reliably tracking in at least 2 sessions in each of these animals.

***Post hoc* neuron identification.** Following 5–7 d after CTB-Alexa647 injection to allow uptake[42], mice were anesthetized (ketamine/xylazine; 100/20 mg per kg body weight) and perfused transcardially with 4% paraformaldehyde in phosphate buffer, pH 7.4. Cortical sections (50 µm) were cut along the imaging plane using a vibratome (VT100; Leica). Images were acquired with a confocal microscope (Fluoview 1000; Olympus) with green (YC-Nano140), red (tdTomato), and infrared (CTB-Alexa647) excitation/emission filters.

Calcium imaging analysis. Two-channel (CFP/YFP) calcium imaging data was imported into MATLAB (Mathworks) for processing. First, background was subtracted on each channel (bottom first percentile fluorescence signal across entire video). Hidden Markov Model line-by-line motion correction was applied to both data channels[43]. Regions of interests (ROIs) corresponding to individual neurons were manually selected from the mean image of a single-trial time series using ImageJ (US National Institutes of Health). Mean pixel value for each ROI was extracted for both channels. Calcium signals were expressed as relative YFP/CFP ratio change $\Delta R/R = (R - R_0)/R_0$. R_0 was calculated for each trial as the bottom eighth percentile of the ratio for the trial. Active neurons were identified by two-way ANOVA with repeated-measures of the neuronal calcium signal against the neuropil signal (significance value, $P < 0.05$). The neuropil is defined as a ROI selected from the entire imaging frame representing non-somatic tissue expressing YC-Nano140 but excluding blood vessels. YC-Nano140 reports a large range of action potential (AP)–evoked neuronal activity with 1AP producing ~2% $\Delta R/R$ peak response[8]. To estimate AP firing-rate changes we deconvolved $\Delta R/R$ calcium transients with a 1AP-calcium transient template (exponential rising and decaying function; previously determined parameters $A_0 = 4.54\%$, $\tau_{onset} = 0.186$ s, $\tau_{decay} = 0.673$ s; ref. 8) using a MATLAB Wiener filter (smoothness parameter = 0.0001). The mean of the pre-touch baseline was subtracted from the deconvolved trace to obtain the change in instantaneous AP firing rate. The integral of the deconvolved trace thus represents the number of extra APs evoked during the trial period.

Animal performance analysis. Animal performance during training was calculated along a sliding window of 40 trials as $d' = Z(\text{Hit}/(\text{Hit}+\text{Miss})) - Z(\text{FA}/(\text{FA}+\text{CR}))$ where $Z(p), p \in [0,1]$, is the inverse of the cumulative Gaussian distribution (FA, false alarm rate; CR, correct rejection rate). For identification of the onset and completion of learning, a learning curve and its confidence intervals was computed for each animal using a state-space smoothing algorithm[11]. The trial representing learning onset represents the trial, in which the lower 95% confidence bound of the estimated learning curve exceeds and remains above 50% correct response probability for the remainder of the experimental time course. The trial representing the completion of learning represents the trial, in which the ideal observer obtained a 95% level of certainty that the animal's performance is better than chance at each trial for the remainder of the experimental time course. For the average pre-stimulus lick rate across training, the mean licking rate across the 2-s period before first texture touch was first calculated for each trial followed by taking the mean value across a sliding window of 40 trials. For the average pre-stimulus whisking amplitude across training, the difference between the mean whisking amplitude for the first and second seconds before first texture touch was first calculated for each trial followed by taking the mean value across a sliding window of 40 trials. Cross-correlation of the resulting vector for pre-stimulus lick rate or whisking amplitude across training was performed against the animal performance vector representing the d' along a sliding window of 40 trials.

Behavior classification. For whisker touch, a binary vector was constructed representing whisker contact periods and down-sampled to the 7-Hz imaging rate. Using MATLAB, cross-correlation of touch vector and cellular calcium signal vectors was performed across the entire imaging session, with all trials concatenated into single vectors with n elements. For two time series vectors x_t and y_t covariance across lags $k = 0, \pm1, \pm2$ frames was calculated as

$$c_{xy} = \begin{cases} 1/n\sum_{t=1}^{n-k}(x_t - \bar{x})(y_{t+k} - \bar{y}) & k = 0,1,2\ldots \\ 1/n\sum_{t=1}^{n+k}(y_t - \bar{y})(x_{t-k} - \bar{x}) & k = -1,-2\ldots \end{cases}$$

The sample cross-correlation (R value) was then computed as

$$R_{xy}(k) = \frac{c_{xy}(k)}{\sigma_x \sigma_y} \quad k = 0, \pm1, \pm2\ldots$$

where σ_x and σ_y denote standard deviation of x_t and y_t, respectively. To determine whether calcium signals of a neuron were significantly correlated to touch above chance levels, we performed a random permutation test by shuffling individual time points along the calcium signal vector across the entire behavior session. The sample cross-correlation was then computed on this shuffled data set and shuffling repeated 1,000 times to obtain a distribution of R values, from which confidence intervals and p-values could be determined for significance tests. Bootstrapping with sample replacement was also performed, randomly replacing calcium transients from individual trials with transients of other trials from the same behavior session. The sample cross-correlation was then computed against the touch vector on this bootstrapped data set. This process was repeated 1,000 times to obtain 95% confidence intervals.

In general, correlations with positive time lags indicate that calcium signals follow touch whereas correlations with negative time lags indicate calcium signals precede touch. The peak R value over the range of time lags analyzed typically correlates to the peak of the calcium transient, as opposed to the calcium signal onset. Touch cells were identified as having a peak positive R value for touch above chance (from random permutation test) between lags $k = 0$ to 4 frames ($t = 0$–571 ms). Active cells with no significant correlation for touch were classified as non-touch. Active cells with a peak negative R-value between lags $k = 0$ to 4 frames or peak positive R-value at $k > 4$ frames or $k < 0$ frames for were also classified as non-touch. Whisking cells were also identified using methods previously described[8], but were classified as non-touch for this study.

To determine the likelihood that the measured distribution of behavior-classified neurons across S2P, M1P and UNL subtypes was above chance, a random permutation test was performed by shuffling the classification labels. For each permutation, the fraction of cells belonging to a particular behavior classification was calculated. This process was repeated 1,000 times to obtain a distribution for each behavior-subtype combination representing the null hypothesis that no behavior-subtype dependencies exist. To compare the measured distribution of classified cells across S2P, M1P and UNL subtypes, bootstrapping with sample replacement of cells with a defined behavior-subtype combination was performed 1,000 times to obtain 95% confidence intervals for each observed combination.

Whisker kinematic analysis. For analysis of kinematic parameters, stick-slip events were identified as previously described[23]. Principal whisker velocity and acceleration were determined by calculating the first and second derivative, respectively, of the time vector representing whisker tip displacement. Slips were defined as events with both high positive acceleration and high absolute velocity, exceeding thresholds corresponding to four s.d. above the means across all measured trials ($\Theta_A = 0.21$ mm ms^{-2} and $\Theta_V = 0.36$ mm ms^{-1}). Whisker curvature change ($|\Delta\kappa|$), reflecting contact forces following touch[44], was measured as the whisker curvature at each time point of touch minus the mean curvature over the 100-ms period before initial touch. Whisker curvature was determined as $\kappa = 1/R$, where R is the radius of a circle, in which the whisker length represents the arc length between the follicle and tip position and in which the direct distance between the follicle and tip position represents the chord. Whisker angle was calculated as the arctangent of $(x_{follicle} - x_{tip})/(y_{follicle} - y_{tip})$ where 0 degrees is orthogonal to the anterior-posterior axis.

Analysis of kinematic-related calcium responses was performed on touch neurons identified in each imaging session. The population touch response per trial was calculated by averaging the calcium responses of identified touch neurons across each cell type. The subsequent trial responses were then sorted

doi:10.1038/nn.4046

according to animal performance level and kinematic parameter. The peak calcium response was calculated as the maximum $\Delta R/R$ value within the first second after initial touch. For cross-correlation analysis of kinematic parameters to calcium response, time vectors of kinematic parameters were first down-sampled to the imaging frame rate. A vector constructed by concatenating the initial 1-s periods after touch (seven frames per trial) across all trials for kinematics was cross-correlated against a similar concatenated vector of the calcium signal representing the average response of all touch neurons of a given subtype. For stick-slip events, cross-correlation was performed on a time vector corresponding to the cumulative number of stick-slip events over the time period. For curvature change, cross-correlation was performed on a time vector representing the cumulative $|\Delta\kappa|_{max}$ at each frame interval. Due to limited imaging speed, slow calcium indicator kinetics, and because L2/3 neuronal activity in S1 is largely devoid of fast touch signals[19,21], measured calcium responses are not likely to represent instantaneous kinematic features. The correlation values obtained represent relative measures of response preferences to these parameters solely to permit a comparison across cell types.

Trial type analysis. The performance of single neurons in discriminating two trial types was assessed using an ROC analysis[21,45]. Classification of decision X (or stimulus X) versus decision Y (stimulus Y) was based on the similarity of the calcium transient in each trial to the mean calcium transient for trial type X compared to trial type Y. Only the first second of the calcium signals following initial texture contact was considered. Each trial was assigned a discrimination variable score (DV) equal to the dot-product similarity to the mean calcium transient for trial type X minus the dot-product similarity to the mean for trial type Y. Thus, for trial type X

$$DV_X = X_i(\bar{X}_{\forall j \neq i} - \bar{Y})$$

and for trial type Y

$$DV_Y = Y_i(\bar{X} - \bar{Y}_{\forall j \neq i})$$

where X_i and Y_i are the single-trial calcium transients for the i-th trial. $\bar{X}$ and $\bar{Y}$ are the mean 1-s calcium transients following initial texture contact for the respective trial type. Trials were classified as belonging to trial type X or Y if DV_X or DV_Y was greater than a given criterion, respectively. To determine the fraction of trials an ideal observer could correctly classify, an ROC curve was constructed by varying this criterion value across the entire range of DV_X or DV_Y. At each criterion value, the probability that a trial of type X exceeded the criterion value was plotted against the probability that a trial of type Y exceeded the criterion value. The area under the ROC curve was then calculated to represent the single-neuron performance (fraction correct) as the fraction of trials correctly discriminated by an ideal observer using the DV.

Neurons discriminating above chance were identified using repeated permutations tests where trial type or stimulus labels were randomly shuffled. For each permutation test, a threshold corresponding to the shuffled distribution 95th percentile was calculated. Neurons, whose performance values were above the mean value of this threshold across 1,000 permutation tests, were considered to be discriminating above chance. For training, ROC analysis was performed along a sliding window of ±150 trials and required more than ten trials each of trial type X and trial type Y. For pre- and post-training sessions, ROC analysis was performed across all trials across the entire session. Discrimination within the trial period was determined by performing ROC analysis at each imaging frame for 1 s before and following touch onset.

To determine the fraction of neurons discriminating above chance across learning, a binary vector indicating discrimination above chance against trial number was generated for all neurons. Each vector was stretched along the time dimension and aligned to a common learning onset and completion across animals so that the fraction of discriminating neurons could be calculated at each normalized time point. To determine the change in discriminative performance across learning, a normalized vector representing the performance value against trial number was generated for each neuron. At each normalized time point, the average performance value was calculated across all cells whose performance value was above chance levels at that time point, minus a baseline value equal to the average performance value at 400 trials before learning onset.

For peak calcium response according to trial type, the population touch response per trial was calculated by averaging the calcium responses of identified touch neurons across each cell type. The subsequent trial responses were then sorted according to animal performance level and trial type. The peak calcium response was calculated as the maximum $\Delta R/R$ value within the first second after initial touch. A bias index indicating a neuron's preference for P100 versus P1200 was calculated as $(P100_{peak} - P1200_{peak})/(P100_{peak} + P1200_{peak})$ such that $P100_{peak}$ and $P1200_{peak}$ represents the average peak calcium response for P100 and P1200, respectively.

Statistical analysis. No statistical methods were used to predetermine sample sizes, but our sample sizes are similar to those reported previously[8]. Data distribution was assumed to be normal but this was not formally tested.

A **Supplementary Methods Checklist** is available.

38. Langer, D. *et al.* HelioScan: a software framework for controlling *in vivo* microscopy setups with high hardware flexibility, functional diversity and extendibility. *J. Neurosci. Methods* **215**, 38–52 (2013).
39. Grewe, B.F., Voigt, F.F., van't Hoff, M. & Helmchen, F. Fast two-layer two-photon imaging of neuronal cell populations using an electrically tunable lens. *Biomed. Opt. Express* **2**, 2035–2046 (2011).
40. Chen, J.L., Pfaffli, O.A., Voigt, F.F., Margolis, D.J. & Helmchen, F. Online correction of licking-induced brain motion during two-photon imaging with a tunable lens. *J. Physiol. (Lond.)* **591**, 4689–4698 (2013).
41. Knutsen, P.M., Derdikman, D. & Ahissar, E. Tracking whisker and head movements in unrestrained behaving rodents. *J. Neurophysiol.* **93**, 2294–2301 (2005).
42. Conte, W.L., Kamishina, H. & Reep, R.L. Multiple neuroanatomical tract-tracing using fluorescent Alexa Fluor conjugates of cholera toxin subunit B in rats. *Nat. Protoc.* **4**, 1157–1166 (2009).
43. Dombeck, D.A., Khabbaz, A.N., Collman, F., Adelman, T.L. & Tank, D.W. Imaging large-scale neural activity with cellular resolution in awake, mobile mice. *Neuron* **56**, 43–57 (2007).
44. Birdwell, J.A. *et al.* Biomechanical models for radial distance determination by the rat vibrissal system. *J. Neurophysiol.* **98**, 2439–2455 (2007).
45. Green, D.M. & Swets, J.A. *Signal Detection Theory and Psychophysics* (Wiley, 1966).